Supplementary Information

Section A: Synthetic dataset creation

The synthetic dataset mimics OA mass spectral analyses of a ToF-ACSM in Zurich. We used source-specific OA mass spectra retrieved from the AMS Spectral database (Ulbrich et al., 2009) and OA source concentration time series generated by the air quality model CAMx (Comprehensive Air Quality Model with Extensions) previously published by Jiang et al. (2019). The represented OA sources are HOA, BBOA, SOA from biogenic emissions (SOAbio), SOA from biomass burning (SOAbb) and SOA from traffic and other anthropogenic sources (SOAtr). Reference profiles selected were: HOA and BBOA from Crippa et al., (2013), SOAtr from Sage et al., (2008), SOAbio represented by a spectrum from Daellenbach et al. 2017 (summer-OOA), and SOAbb represented by a spectrum from Daellenbach et al. 2017 (winter-OOA). For every OA source the mass spectrum is multiplied with its concentration time series. In a first step, the concentrations of the species (m/zs) were calculated by multiplying the OA sources' mass spectra (normalised to 1) obtained from the AMS Spectral Database (Ulbrich et al., 2009) with its concentration time series of each from the CAMx Model and summing the five matrices up. The result is the mass spectral data matrix (I_{diff}). We assume that the ToF-ACSM detects 200 ions/s per µg/m^3 OA which allows for computing ion counts at a single organic m/z.

The error matrix was computed following the same steps as for real-world data. Since the OA measurements are computed as the difference between analyses of air+particle (Iopen) and air (Iclosed), these measurements are the basis of the uncertainty estimates. We assume that baseline spectrum (Ibaseline), and the intensity of closed spectrum (Iclosed) are constant over time, 1 hour long timestamps and airbeam correction constant and equal to 1.

The error related to Iclosed is described as:

$$e_{closed,ij} = \sqrt{(I_{closed,ij} + I_{baseline,ij}) \cdot \frac{t_{closed}}{\sqrt{28}}} \quad (2)$$

The error related to Iopen is described as:

$$e_{open,ij} = \sqrt{(I_{open,ij} + I_{baseline,ij}) \cdot \frac{t_{open}}{\sqrt{28}}} \quad (3)$$

With

$$t_{open} = t_{closed} = 90 \cdot 18\,(s) \quad (4)$$

and

$$I_{open} = I_{closed} + I_{diff} \quad (5)$$

Sorry

Thus the error related to Idiff is:

$$e_{ij} = max\left(1.2 \cdot \frac{1}{90 \cdot 18} \cdot \sqrt{\frac{28}{m/z}} \cdot \sqrt{{e_{open,ij}}^2 + {e_{closed,ij}}^2}\ , \frac{1}{1620}\right)\ (ions/s) \quad (6)$$

$$e_{ij}\ (\mu g/m3)) = \frac{1}{200\ (ions/s/\mu g/m3)} \cdot\ e_{ij}\ (ions/s) \quad (7)$$

Section B: Figures and Tables.

Table S1. PMF datasets characteristics of the multi-site study.

Site	PMF m/z spectra	Publication	Rolling window	CE	Reference profiles	Pieber effect
BCN-PR	12-120 (92)	(Via et al., 2021)	14	fPhase	HOA, COA: Crippa et al., 2013 BBOA: Ng et al., 2010	No
CAO-AMX	13-100 (72)	-	14	0.5	HOA: Crippa MEGAPOLI BBOA: derived from this study.	No
DUB	16-100 (72)	Lin et al., (in prep)	14	1	HOA: Crippa et al., 2013 Peat, Wood, Coal: Lin et al., 2017	No

ATOLL	13-100 (72)	Chebaicheb et al., (in prep.)	14	fPhase	HOA, BBOA before seasonal bootstrap: Crippa et al. 2013 HOA, BBOA final solution: winter seasonal results	No
MGD	16-100 (70)	(Chen et al., 2021)	14	0.45	HOA before bootstrap: Crippa et al., 2013 HOA, BBOA final solution: seasonal winter solution	No
INO	13-120 (92)	Vasilescu et al., (in prep.)	14	0.5	HOA: Marmureanu et al., 2020; Vasilescu et al., (in prep.) BBOA: Ng et al., 2011	No

MRS-LCP	12-214 (185)	Chazeau et al., (in prep.)	14	fPhase	HOA: Ng et al, 2011 COA: Crippa et al., 2013 Sh-IndOA: SO2 TS from MRS-LCP site	Yes
SIR	13-100	(Zhang et al., 2019)	28	0.5	HOA: Crippa et al., 2013 BBOA: Frohlich et al., 2015	No
TAR	12-100 (73)	-	28	fPhase	HOA: Crippa et al., 2013 BBOA: seasonal winter solution	No

Table S2. Ancillary instrumentation at each site used for source apportionment.

Site	**Measurement**	**Instrumentation**
BCN-PR	NO_x	Thermo Scientific, Model 43i
CAO-AMX	NO_x	Ecotech 9841T
DUB	NO_x	https://aqicn.org/city/ireland/rathmines/
ATOLL	NO_x	Not available.

MGD	NO_x	https://aqicn.org/city/switzerland/magadino-cadenazzo/
INO	NO_x	Thermo Scientific model 42i
MRS-LCP	NO_x	NOx analyser model 200E (Teledyne)
	SO_2	SO2 analyser model 100E (Teledyne)
	UFP number	UFP monitor 3031 (TSI)
	Particle Size Distribution	MPSS (GRIMM)
SIR	NOx	T200UP Teledyne
TAR	NOx	Horiba APNA-360
	$PM_{2.5}$ and PM_{10}	MetOne BAM1020

Table S3. (a) Reference profiles and a-random ranges used in PMF running ofthe synthetic dataset. (b) Criteria and thresholds for run selection in the synthetic dataset.

(a)	Reference profile	Minimum a value	Maximum a-value	a-value step	
				Rolling	Seasonal
HOA	(Crippa et al., 2013)	0.1	0.2	0.05	0.05

BBOA	(Ng et al., 2011)	0.1	0.3	0.05	0.05

42

(b)	Criteria	Threshold	
		Seasonal	Rolling
HOA	Diel Squared-Pearson correlation with EC.	R^2>0.35 and p<0.05	R^2>0.50 and p<0.05
HOA	Diel Squared-Pearson correlation with NO_2.	R^2>0.2 and p<0.05	R^2>0.4 and p<0.05
BBOA	Explained variation of f60.	>0.20	>0.20
BBOA	Ratio of time series factor variable 60 and 44.	>0.30	>0.30
LO-OOA	Profile f43 (for differentiation).	All	>0.02
MO-OOA	Profile f44 (for differentiation).	All	>0.02

43

44 **Table S4. Squared Pearson correlation coefficient and orthogonal distance fit slopes and intercepts for the OA vs.**
45 **apportioned OA comparison. In columns, the period along which these calculations are performed and averaged and**
46 **the two SA methods on trial, *rolling* (R) and *seasonal* (S).**

		Rolling	Seasonal

Site	Resolution	R^2	ODR fit	R^2	ODR fit
BCN-PR	Period	0.97	0.99x-0.04	0.97	1.00x-0.05
	Season	1.00	1.00-0.08	0.87	0.92x+0.035
	Fortnight	1.00	0.98+0.02	0.98	1.00x-0.01
	Day	1.00	0.99x-0.02	0.99	1.00x-0.05
CAO-AMX	Period	0.99	0.97x+0.14	0.99	0.96x+0.010
	Season	0.95	1.09x-0.24	1.00	0.97+0.05
	Fortnight	0.98	0.99x+0.08	0.97	1.02+0.07
	Day	0.99	0.97x+0.13	1.00	0.95x+0.08
DUB	Period	1.00	1.00x-0.01	1.00	0.99x+0.01
	Season	1.00	1.00x-0.02	1.00	1.01x-0.04
	Fortnight	1.00	1.00x-0.00	1.00	1.00x-0.00
	Day	1.00	0.99x-0.00	1.00	0.99+0.01
ATOLL	Period	0.99	1.00x+0.02	0.98	1.00x-0.02
	Season	1.00	1.00x-0.01	1.00	1.00x-0.00
	Fortnight	1.00	1.00x-0.02	1.00	1.00x-0.05
	Day	1.00	1.00x-0.02	1.00	1.00x-0.04
MGD	Period	0.99	1.00x+0.02	0.98	1.00-0.00
	Season	1.00	1.00x+0.02	0.99	1.01x-0.15
	Fortnight	1.00	1.00x-0.00	0.99	1.01x-0.12
	Day	1.00	1.00x-0.02	1.00	1.01x-0.06
INO	Period	0.88	1.07x-0.77	0.98	1.09x-1.14

	Season	1.00	0.99x+0.15	0.97	0.98x+0.15
	Fortnight	1.00	1.00x+0.58	0.97	1.07x-0.58
	Day	0.99	1.04x-0.50	0.98	1.06x+0.92
MRS-LCP	Period	1.00	1.00x-0.03	0.99	1.03x+0.16
	Season	1.00	1.00x-0.01	1.00	0.97x+0.10
	Fortnight	1.00	1.00x-0.04	1.00	1.01x-0.02
	Day	0.99	1.01x+0.03	0.99	1.02x-0.05
SIR	Period	1.00	0.95x+0.05	0.96	0.95x+0.02
	Season	1.00	0.93x+0.15	1.00	0.94x+0.15
	Fortnight	1.00	0.94x+0.08	1.00	0.95x+0.04
	Day	1.00	0.95x+0.05	0.99	0.96x+0.00
TAR	Period	1.00	0.92x+0.05	1.00	0.92x+0.05
	Season	1.00	0.92x+0.04	1.00	0.93x+0.01
	Fortnight	1.00	0.93x+0.02	1.00	0.93x+0.00
	Day	1.00	0.93x+0.03	1.00	0.93x+0.02
SYN	Period	1.00	1.14x-0.08	1.00	1.14x-0.07
	Season	1.00	1.15x-0.12	1.00	1.14x-0.12
	Fortnight	1.00	1.14x-0.08	1.00	1.14x-0.08
	Day	1.00	1.36x-0.07	1.00	1.36x-0.07

47

48

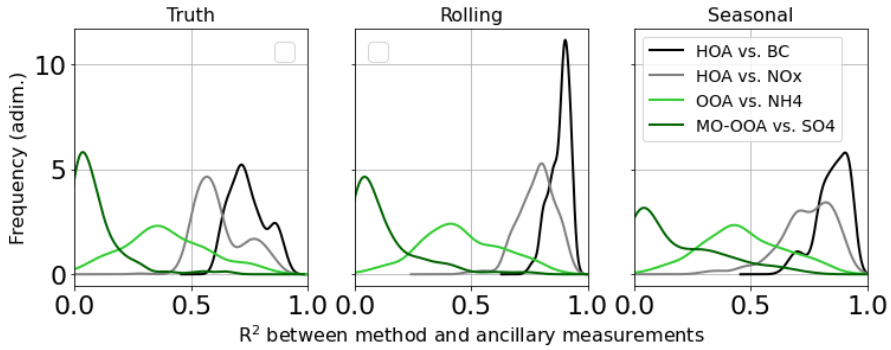

Figure S1. Histogram of the difference of *rolling* minus *seasonal* of the Pearson-squared correlation coefficient of the synthetic OA factors and their potential markers.

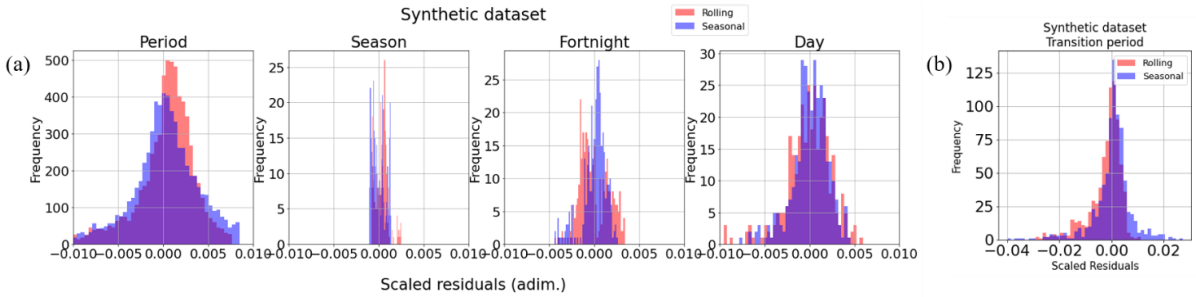

Figure S2. Scaled residuals distribution (a) for the whole period and 90-days, 14-days and 1-day resolutions. (b) transition periods. Number of bins is 50 in all cases.

Table S5. Welch's t-test rejections (marked with a bullet-dot) over the p<0.05 threshold value for all sites, factors and time spans (P: period; S: season; F: fortnight; D: day). Note that for 'other POA' the 'ALL' site does not show information, as they are shown at their respective sites. Hyphens and slashes flag those cells which have no representation in one site (this is, that site does not have this factor) and those which have more than one factor in a cell, respectively.

Welch's t-test	HOA				BBOA				Other POA				LO-OOA				MO-OOA				OOA				OA			
	P	S	F	D	P	S	F	D	P	S	F	D	P	S	F	D	P	S	F	D	P	S	F	D	P	S	F	D
BCN-PR	*	*	*			*			*	*	*	*	*				*				*							
CAO-AMX	*	*			*	*	*	*	-	-	-	-	*	*	*	*	*	*	*	*	*					*	*	*

DUB					-	-	-	-	//	//	//	//	*	*			*											
ATOLL	*	*	*	*	*	*	*	*	-	-	-	-	*		*		*	*	*	*	*	*	*	*	*	*	*	
MGD	*	*	*	*	*	*	*	*	*	*	*	*	*				*	*	*	*	*	*	*	*	*	*	*	*
INO	*	*	*		*				-	-	-	-	*	*	*	*	*	*	*									
MRS-LCP	*	*	*		*	*	*	*	/*	*/	*/	/	*	*	*	*	*	*	*	*	*					*		
SIR	*	*	*	*	*	*			-	-	-	-	*	*	*	*	*	*	*	*	*	*	*		*			
TAR		*	*						-	-	-	-	*	*	*		*											
ALL	*	*	*	*	*				-	-	-	-	*				*	*	*	*	*	*	*	*	*	*	*	*

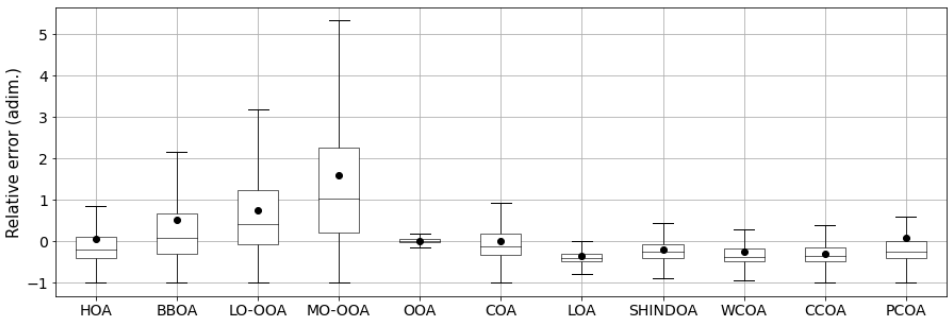

Figure S3. Boxplots of relative error *rolling – seasonal*, i.e., the difference between methods divided by the mean of the concentrations between *seasonal* and *rolling*.

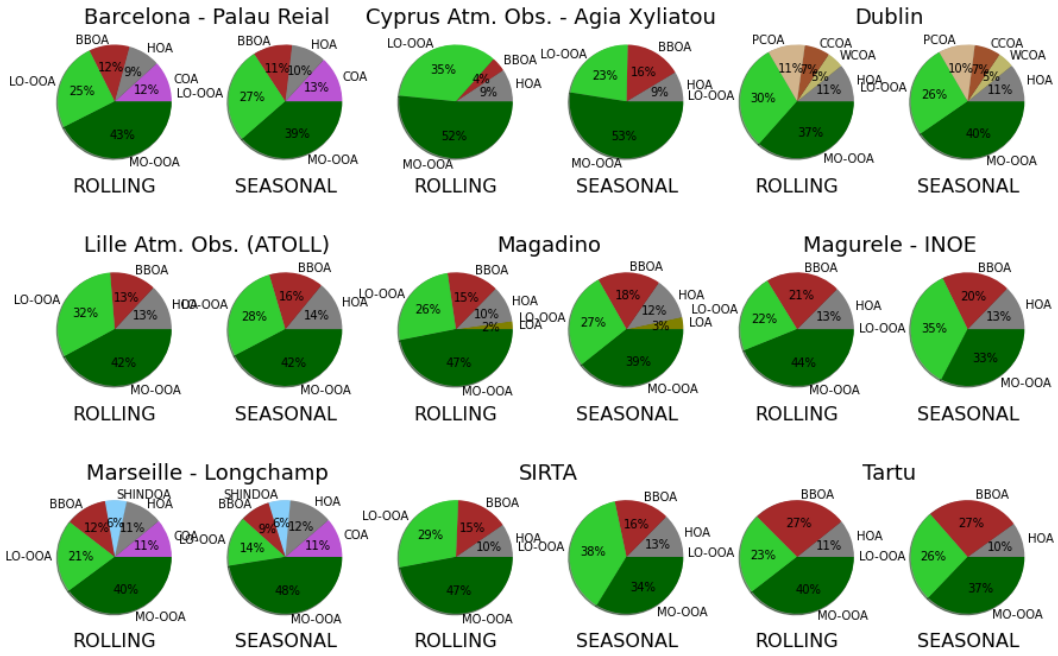

Figure S4. Pie plots for rolling and seasonal results for each site in the comparison.

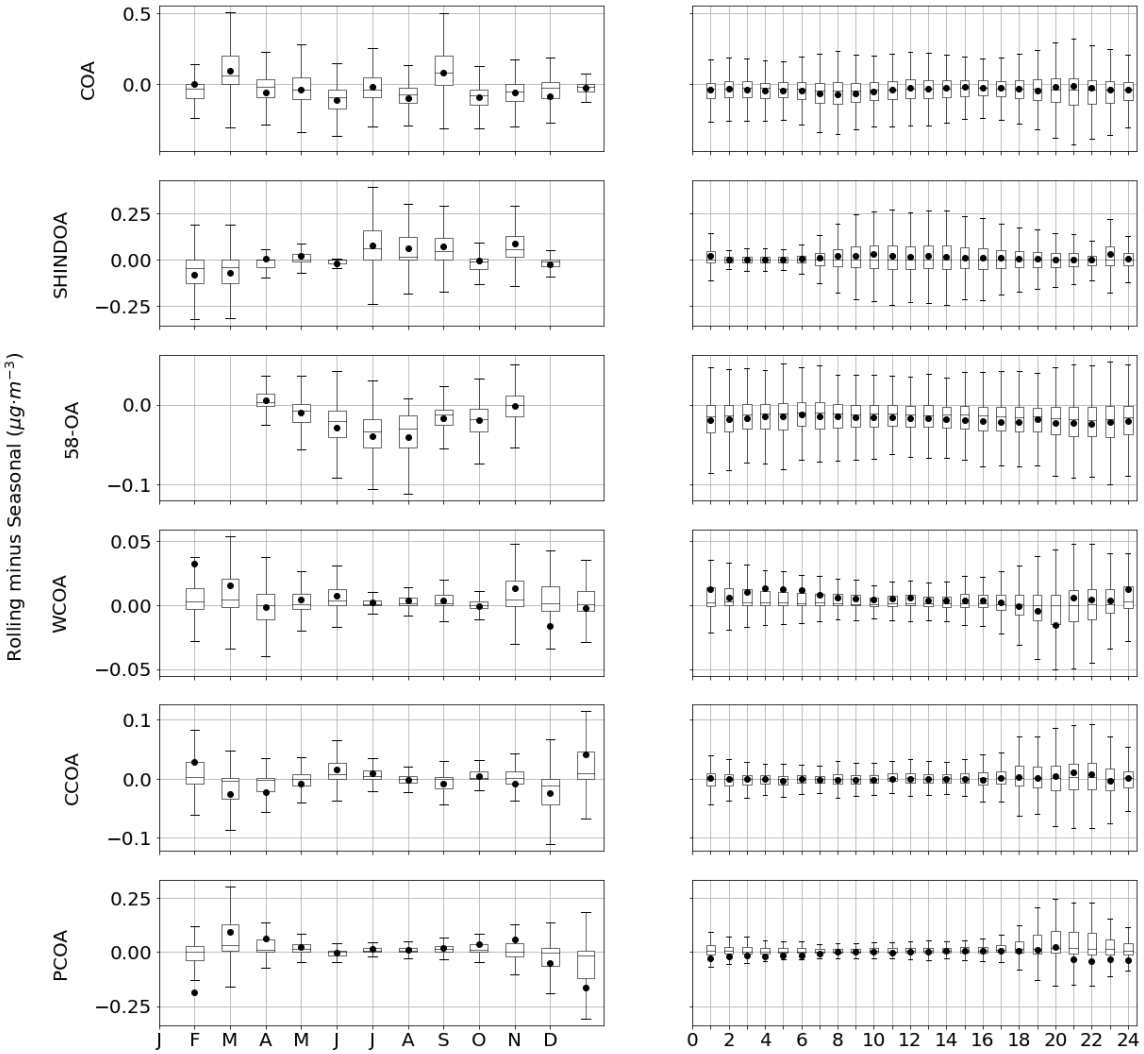

Figure S5. Boxplots of *rolling – seasonal* factor concentrations per month and hour of the factors which are not present in all sites. Boxes show the Q1-to-Q3 range and the median, and whiskers extend up to the range of the data and round markers show the means.

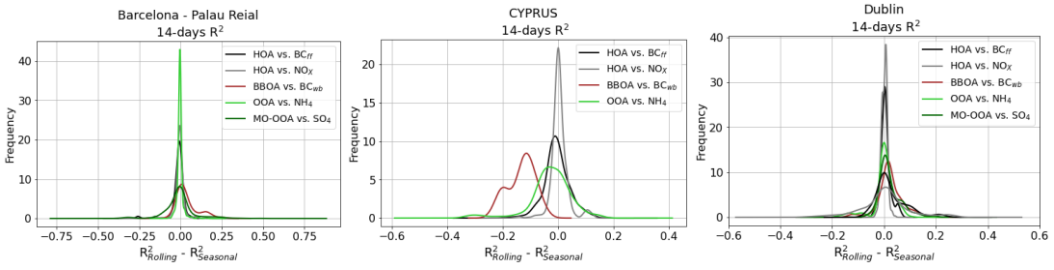

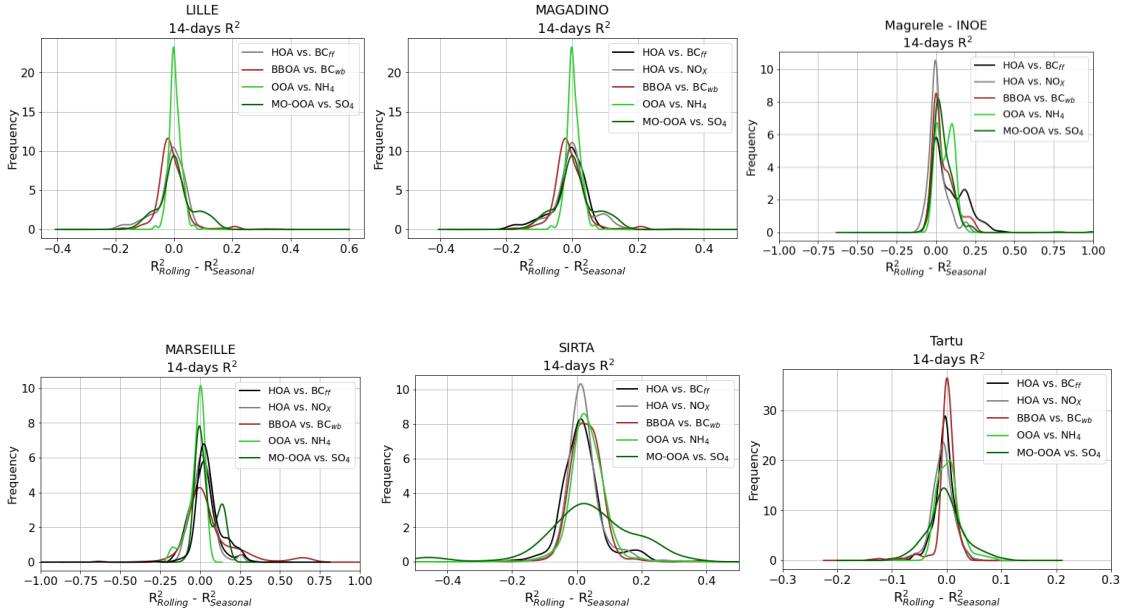

Figure S6. Kernel density estimation of difference between rolling and seasonal R^2 to correlated measurements.

Table S6. Pearson correlation coefficients between factors and co-located measurements for the *rolling* and *seasonal* during transition periods from one season to the following in each site and as a whole. Whole refers to the correlation between factors and markers of the concatenated time series of all sites.

R^2 in transition periods	HOA vs. BC_{ff}		HOA vs. NO_x		BBOA vs. BC_{wb}		MO-OOA vs. SO_4^{2-}		OOA vs. NH_4^+	
	R	S	R	S	R	S	R	S	R	S
BCN-PR	0.75	0.76	0.62	0.63	0.13	0.05	0.31	0.27	0.59	0.62
CAO-AMX	0.21	0.14	0.05	0.05	0.04	0.26	0.49	0.56	0.52	0.52
DUB	0.88	0.86	0.36	0.35	-	-	0.4	0.24	0.66	0.58
ATOLL	0.47	0.52	-	-	0.18	0.17	0.00	0.01	0.00	0.00

MAG	0.32	0.30	0.42	0.43	0.86	0.84	0.43	0.50	0.48	0.48
INO	0.12	0.08	0.24	0.12	0.65	0.57	0.21	0.17	0.61	0.40
MRS-LCP	0.54	0.54	0.56	0.54	0.88	0.54	0.3	0.12	0.57	0.61
SIRTA	0.44	0.43	0.48	0.43	0.68	0.74	0.48	0.25	0.56	0.50
TAR	0.27	0.25	0.31	0.31	0.73	0.74	0.12	0.27	0.21	0.15
Whole	0.49	0.47	0.25	0.15	0.49	0.51	0.26	0.27	0.44	0.39

78

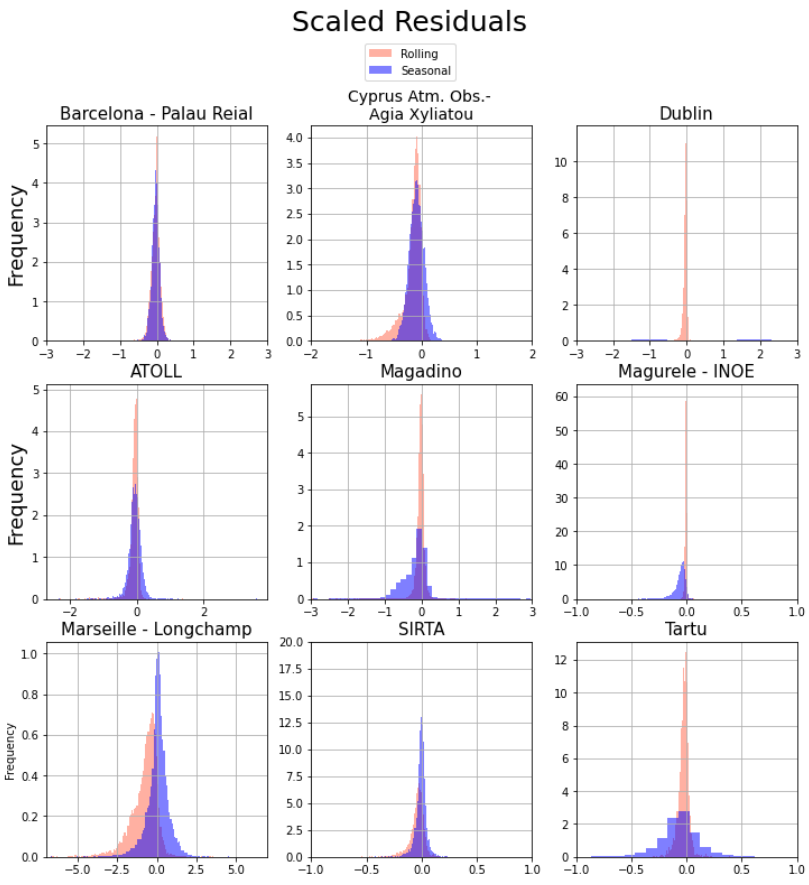

79

Figure S7. Scaled residuals histograms for all sites.

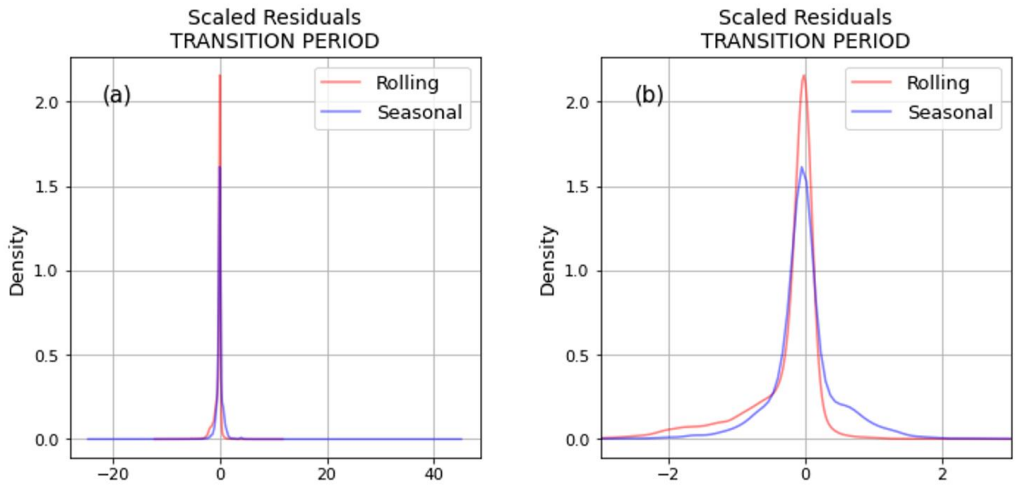

Figure S8. Kernel density estimation of scaled residuals of the *rolling* and *seasonal* solution in the transition periods between seasons where (b) represents a zoom of figure (a).

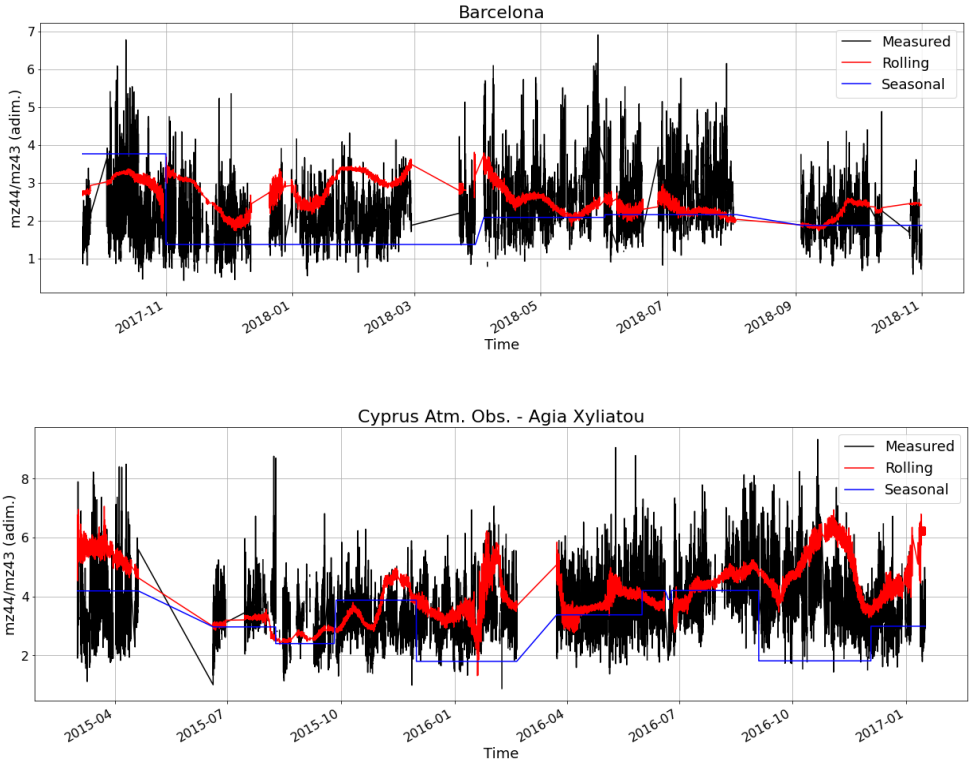

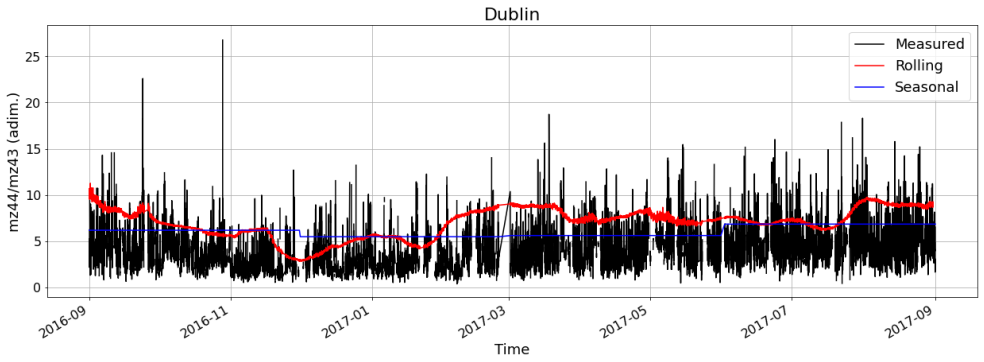
Dublin
Measured
Rolling
Seasonal
mz44/mz43 (adim.)
Time

88

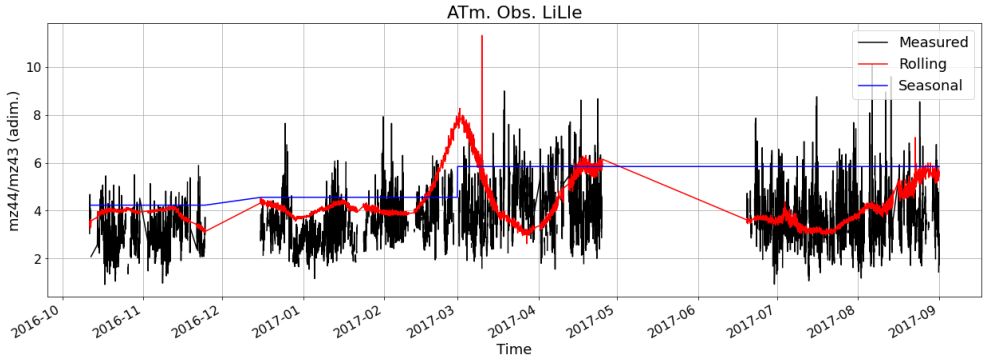
ATm. Obs. LiLle
Measured
Rolling
Seasonal
mz44/mz43 (adim.)
Time

89

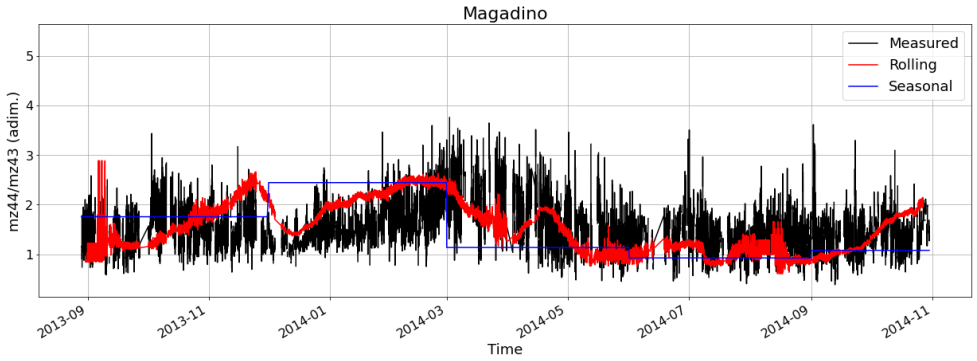
Magadino
Measured
Rolling
Seasonal
mz44/mz43 (adim.)
Time

90

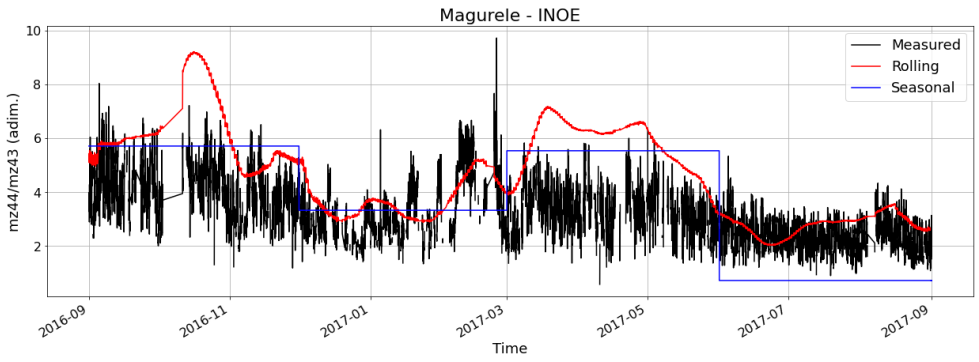
Magurele - INOE
Measured
Rolling
Seasonal
mz44/mz43 (adim.)
Time

91

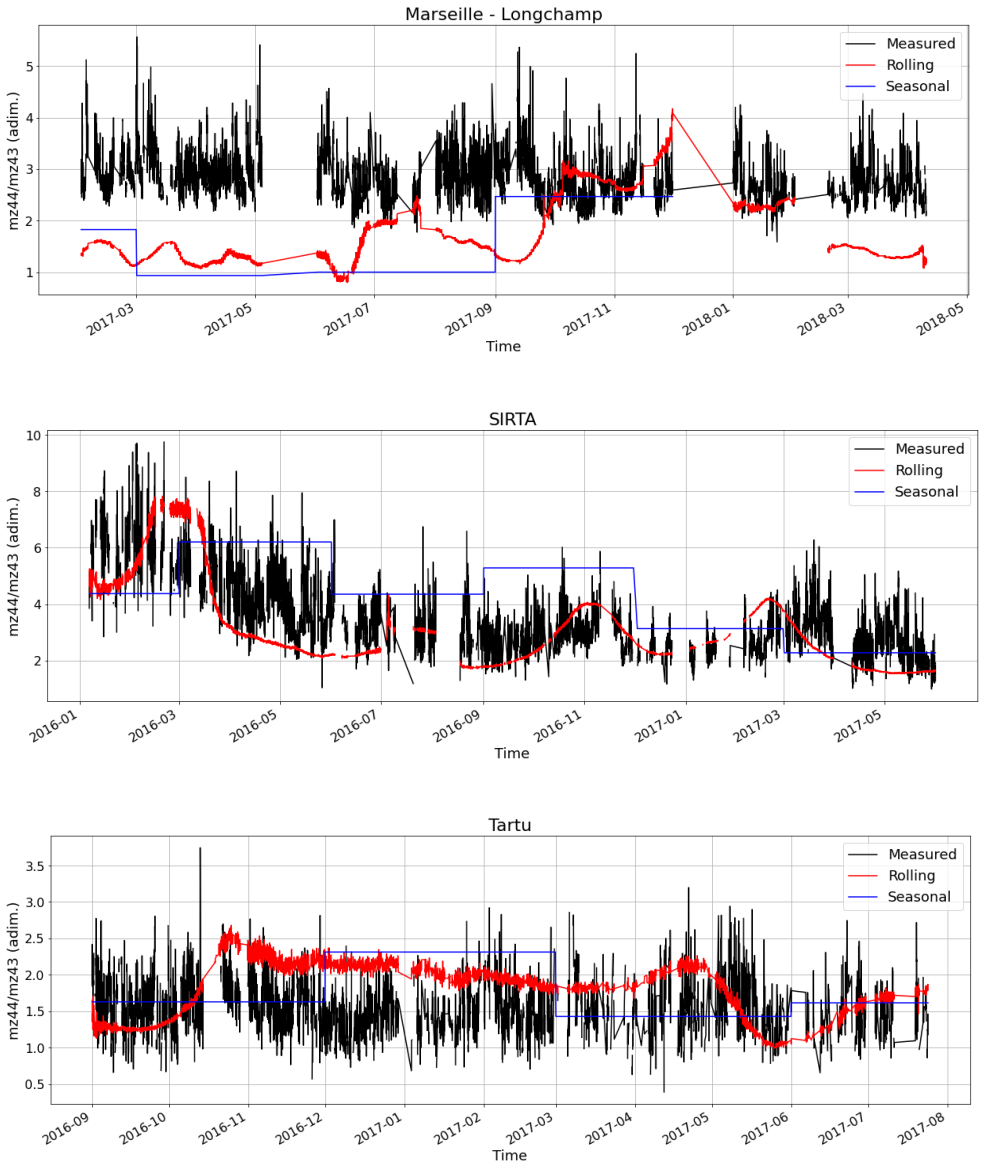

Figure S7. Time series of the *m/z44*-to-*m/z43* ratios for raw time series and SOA profiles for all the sites.

References

Chen, G., Sosedova, Y., Canonaco, F., Fröhlich, R., Tobler, A., Vlachou, A., Daellenbach, K., Bozzetti, C., Hueglin, C., Graf, P., Baltensperger, U., Slowik, J., El Haddad, I. and Prévôt, A.: Time dependent source apportionment of submicron organic aerosol for a rural site in an alpine valley using a rolling PMF window, Atmos. Chem. Phys. Discuss., 43, 1–52, doi:10.5194/acp-2020-1263, 2021.

Crippa, M., Decarlo, P. F., Slowik, J. G., Mohr, C., Heringa, M. F., Chirico, R., Poulain, L., Freutel, F., Sciare, J., Cozic, J., Di Marco, C. F., Elsasser, M., Nicolas, J. B., Marchand, N., Abidi, E., Wiedensohler, A., Drewnick, F.,

Schneider, J., Borrmann, S., Nemitz, E., Zimmermann, R., Jaffrezo, J. L., Prévôt, A. S. H. and Baltensperger, U.: Wintertime aerosol chemical composition and source apportionment of the organic fraction in the metropolitan area of Paris, Atmos. Chem. Phys., 13(2), 961–981, doi:10.5194/acp-13-961-2013, 2013.

Daellenbach, K. R., Uzu, G., Jiang, J., Cassagnes, L. E., Leni, Z., Vlachou, A., Stefenelli, G., Canonaco, F., Weber, S., Segers, A., Kuenen, J. J. P., Schaap, M., Favez, O., Albinet, A., Aksoyoglu, S., Dommen, J., Baltensperger, U., Geiser, M., El Haddad, I., Jaffrezo, J. L. and Prévôt, A. S. H.: Sources of particulate-matter air pollution and its oxidative potential in Europe, Nature, 587(7834), 414–419, doi:10.1038/s41586-020-2902-8, 2020.

Dee, D. P., Uppala, S. M., Simmons, A. J., Berrisford, P., Poli, P., Kobayashi, S., Andrae, U., Balmaseda, M. A., Balsamo, G., Bauer, P., Bechtold, P., Beljaars, A. C. M., van de Berg, L., Bidlot, J., Bormann, N., Delsol, C., Dragani, R., Fuentes, M., Geer, A. J., Haimberger, L., Healy, S. B., Hersbach, H., Hólm, E. V., Isaksen, L., Kållberg, P., Köhler, M., Matricardi, M., Mcnally, A. P., Monge-Sanz, B. M., Morcrette, J. J., Park, B. K., Peubey, C., de Rosnay, P., Tavolato, C., Thépaut, J. N. and Vitart, F.: The ERA-Interim reanalysis: Configuration and performance of the data assimilation system, Q. J. R. Meteorol. Soc., 137(656), 553–597, doi:10.1002/qj.828, 2011.

Jiang, J., Aksoyoglu, S., El-Haddad, I., Ciarelli, G., Denier Van Der Gon, H. A. C., Canonaco, F., Gilardoni, S., Paglione, M., Minguillón, M. C., Favez, O., Zhang, Y., Marchand, N., Hao, L., Virtanen, A., Florou, K., O'Dowd, C., Ovadnevaite, J., Baltensperger, U. and Prévôt, A. S. H.: Sources of organic aerosols in Europe: A modeling study using CAMx with modified volatility basis set scheme, Atmos. Chem. Phys., 19(24), 15247–15270, doi:10.5194/acp-19-15247-2019, 2019.

Ng, N. L., Canagaratna, M. R., Jimenez, J. L., Chhabra, P. S., Seinfeld, J. H. and Worsnop, D. R.: Changes in organic aerosol composition with aging inferred from aerosol mass spectra, Atmos. Chem. Phys., 11(13), 6465–6474, doi:10.5194/acp-11-6465-2011, 2011.

Skamarock, W. C. and Klemp, J. B.: A time-split nonhydrostatic atmospheric model for weather research and forecasting applications, J. Comput. Phys., 227(7), 3465–3485, doi:10.1016/j.jcp.2007.01.037, 2008.

Ulbrich, I. M., Canagaratna, M. R., Zhang, Q., Worsnop, D. R. and Jimenez, J. L.: Interpretation of organic components from Positive Matrix Factorization of aerosol mass spectrometric data, Atmos. Chem. Phys., 9(9), 2891–2918, doi:10.5194/acp-9-2891-2009, 2009.

Via, M., Minguillón, M. C., Reche, C., Querol, X. and Alastuey, A.: Increase in secondary organic aerosol in an urban environment, Atmos. Chem. Phys., 21(10), 8323–8339, doi:10.5194/acp-21-8323-2021, 2021.

Zhang, Y., Favez, O., Petit, J. E., Canonaco, F., Truong, F., Bonnaire, N., Crenn, V., Amodeo, T., Prévôt, A. S. H., Sciare, J., Gros, V. and Albinet, A.: Six-year source apportionment of submicron organic aerosols from near-continuous highly time-resolved measurements at SIRTA (Paris area, France), Atmos. Chem. Phys., 19(23), 14755–14776, doi:10.5194/acp-19-14755-2019, 2019.